1st Croatian Conference on Earthquake Engineering
1CroCEE
22-24 March 2021 Zagreb, Croatia

DOI: https://doi.org/10.5592/CO/1CroCEE.2021.157

System-level seismic fragility assessment of multispan continuous integral abutment bridges

Benazir Ahmed[1], **Kaustubh Dasgupta**[2]
[1] *Ph.D.*, Indian Institute of Technology Guwahati, *benazir@iitg.ac.in*
[2] *Associate Professor*, Indian Institute of Technology Guwahati, *kd@iitg.ac.in*

Abstract

Generation of Fragility Curves (FCs) forms the primary basis for seismic vulnerability assessment of structures within a probabilistic framework, which can effectively aid in seismic damage mitigation. This paper presents the system-level FCs generated for a class of reinforced concrete integral abutment bridges, in succession to the component-level FCs developed for the damageable components of the bridge class, namely piers, elastomeric bearings with dowel bars, abutment-backfill system and pile-soil system. System-level FCs have not been studied extensively and while incorporating explicitly the contributions of different components. From the evaluated probabilistic component-level seismic demand data, demand correlation coefficient between every two components at the respective ith Damage State (DS) rank is computed. The joint demand cumulative probability distribution surface is derived using the correlation matrix and the demand distributions at each DS, while the evaluated probabilistic seismic DS capacities of the individual components are considered to be mutually independent. Using Latin Hypercube sampling technique on the joint demand surface and the individual component capacities, the generated sample values for the Joint Demands (JDs) are randomly paired with those for the Capacity Quartets (CQs). Probability of failure of the Bridge System (BS) is computed as the ratio of the cases (JD-CQ pairs) wherein the BS DS is reached (if at least one of the capacity values is exceeded by one or all the demand values in a pair) to the total cases. Computation is repeated at each increasing value of the adopted earthquake Intensity Measure (IM) and for all the DSs to obtain the BS FCs. BS at a DS rank is found more vulnerable than the individual components at the respective same DS ranks. BS at DSs of higher ranks than those of the individual components shows more or less vulnerabilities upto certain IM ranges and vice versa beyond as compared to the individual components.

Key words: Demand Correlation Coefficient, Correlation Matrix, Joint Demand Distribution Surface, Latin Hypercube Sampling Technique, System-Level Fragility

1 Introduction

Past earthquakes have demonstrated bridges to be vulnerable to seismic damages and failure; non-functionality causes disruption to social-economic as well as emergency rescue and recovery activities. This has led to the seismic vulnerability assessment of bridges becoming a major research area in earthquake engineering. Fragility Curves (FCs), as its output within a probabilistic perspective, are essential for reasonable decision making on structural designs, retrofits, repairs and damage mitigations [1]; it also enables comparison of various bridge types [2]. The present study aims to generate the FCs for the overall Bridge System (BS) conforming to a class of Integral Abutment Bridges (IABs).

Seismic vulnerability of the BS is contributed by the individual vulnerability effects of its components; it is strongly affected by the coupling between simultaneously developing various damage modes in different components [3]. However, many of the previous studies like [4-8] have represented BS fragility in terms of the seemingly most vulnerable component, such as the columns. BS is more fragile than any of the individual components and ignoring their contributions can lead to misrepresentation of the BS fragility and result in errors as large as 50 % at higher DSs [9].

Thus, some research studies have estimated the BS fragility at a particular DS by combining the individual component fragilities, with the convenience of treating it as a series or a parallel combination, as any or all of the components reach the respective DSs of the same rank correspondingly. In reality, the responses of the components are often correlated with each other to a certain extent and the fragility estimated will be in between the bounds corresponding to the total correlation and complete independence associated with both the series and parallel assumptions for the BS. Nevertheless, the first order bounds considering the series system were adopted by [2]. Second-order reliability was adopted by [10] where some correlation was evaluated and found to yield narrower bounds.

Other than the above approaches, [11] evaluated the BS fragilities considering the composite behaviour of the component DSs, which were assigned weightages based on their relative importance. [12] defined the BS performances based on traffic capacity reduction against the post event component damages for the evaluation. [13] generated the joint demand surface based on correlations among the demands of the bridge components and employed the Monte Carlo simulation on it and as well as on the mutually independent capacities, for evaluating the BS fragilities; later adopted by [14, 15]. To have similar functionality and repair consequences at the BS level, [16], while adopting the approach of [13], classified the bridge components into primary (contribute to all the BS DSs and affect the bridge vertical stability and load carrying capacity) and secondary (contribute to the initial BS DSs and cause traffic restriction) ones. This principle was followed by [17] and so has been followed in the present study.

2 Seismic modeling, capacity and demand evaluation for the iab class

The IAB class in the study (Fig. 1) consists of a multispan continuous Reinforced Concrete (RC) deck with prestressed concrete I-girders, supported on elastomeric rubber bearings. Each bearing has two steel dowel bars passing through it which are embedded into the cap beam and loosely inserted into the underside of the girder diaphragm. The bearings in turn rest on RC multicolumn bents and integral abutments with dense sandy backfill. The bents and the abutments are supported on groups of piles and single rows respectively, of fixed-headed piles in loose sand.

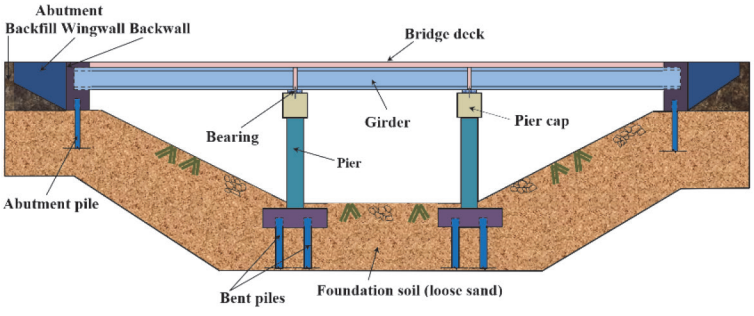

Figure 1. A typical IAB configuration in the study

Employing the Latin Hypercube Sampling Technique (LHST) on the ranges of the probability distributions of the structural and geotechnical parameters, 144 samples for the BS are generated. The numerical models are developed, based on the structural components modeling analogy [18], wherein the BS is modeled as a spline, with *elasticBeamColumn* elements supported on a series of *ZeroLength* springs in OpenSees [19] representing the lateral capacity curves of the IAB components, at the respective locations. These curves are generated through the appropriate analytical models developed for (a) pier in OpenSees, (b) Pile-Soil System (PSS) while linking the finite element model analysis of the PSS in OpenSees with the pile-soil interaction model [20], (c) bearing in the study itself, and (d) Abutment-Backfill System (ABS) while simulating the abutment-backfill interaction based on [21]. A typical fibre section of the pier element, the output lateral force deformation curves for pier and bearing constituents are shown in Figs. 2(a), 2(b) and 2(c) respectively.

Analyses of the respective damage models (developed in [22]) of the components for the corresponding samples, yield the Limit State Threshold (LST)) (denoted as LST1, LST2, LST3 and LST4 against the first four DSs) data against the respective DS (denoted as DS1, DS2, DS3 and DS4 against the four DSs) capacities (*C*s). These are characterised in terms of probability distributions; one such distribution with respect to PSS DS2 is shown in Fig. 2(d). Seismic demand (*D*) against each component DS is assessed, while extending the inverse application of the adaptive capacity spectrum method [23], with

respect to the earthquake Intensity Measures (IMs) as the Peak Ground Acceleration (PGA) and the spectral acceleration at 0.7s S_a(0.7s) based on the near average values of the time periods for the BS samples herein, from damage initiation till collapse). The demand data is obtained from the analyses of all the BS samples, against each of the specified IM values within 0 to 1.8g (to which the PGA and S_a(0.7s) values of the input ground motions are scaled) of all the ground motions. One such distribution is shown in Fig. 2(e) against the bearing DS4 with respect to S_a(0.7s) value of 0.1g. The study employs nine ground motions selected over wide ranges of frequency contents; one such 5 % damped ground motion acceleration-time period response spectrum is shown in Fig. 2(f).

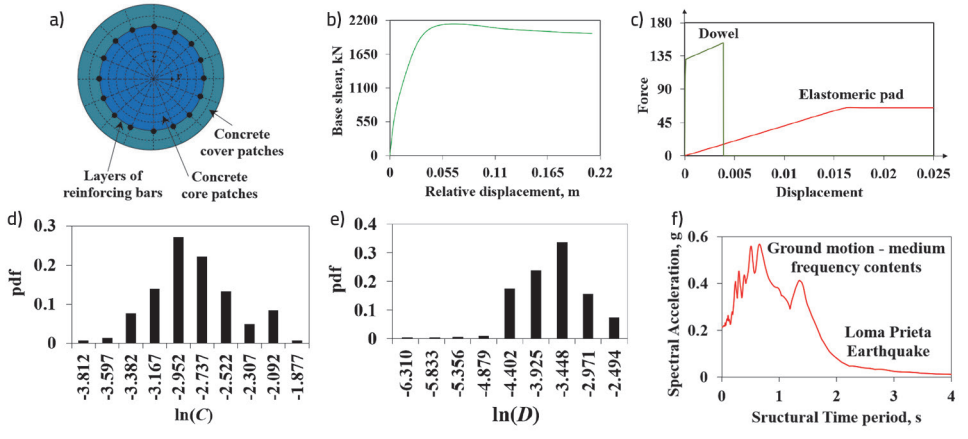

Figure 2. a) A pier fibre section; lateral capacity curves for b) pier and c) bearing constituents; data distributions of d) capacity and e) demand; f) ground motion response spectrum

3. Generation of the Bridge System Fragility Curves

BS FCs in the present study are generated, in succession to the component-level FCs using the evaluated respective *C* and *D* distributions, as discussed in the following subsections:

3.1 Definition of the BS DSs

Four BS DSs are considered (with the LSTs denoted as BS-LST1, BS-LST2, BS-LST3 and BS-LST4), based on the mapping at the system level, of the different component-level DSs [16] (with the LSTs denoted as PC-LST1, PC-LST2, PC-LST3 and PC-LST4 for primary components; and as SC-LST1, SC-LST2, SC-LST3 and SC-LST4 for secondary components). DS descriptions and the mapping are elaborated in a flowchart in Fig. 3. While developing the damage models for the components, DS of a component with the assigned rank is designed such that it has the same functionality consequences at the BS level with respect to the same DS rank. Hence, the BD DS1; DS2; DS3; and DS4 are

defined by the mapped contributions of the DS1s of PSS, ABS, bearing and pier; DS2s of PSS, ABS, bearing and pier; DS3s of ABS, bearing and pier; and DS4s of bearing and pier respectively.

3.2 Evaluation of the joint demand cumulative distribution surface of the IAB components

Seismic demands of the components being correlated, BS fragility evaluation requires derivation of the joint demand cumulative probability distribution surface (JDS). Thus, the correlation coefficient $\rho_{i,p\text{-}q}$ between every two (p^{th} and q^{th}) components (PSS, ABS, bearing and pier, denoted as '*pl*', '*ab*', '*br*' and '*pr*' respectively) at i^{th} DS rank is computed from the respective ln(D) data (1296 values) (i.e., ln($D_{i,p}$) and ln($D_{i,q}$), as in Eq. (1), and listed in Table 1 for all the cases. Employing $\rho_{i,p\text{-}q}$ s and standard deviations of ln($D_{i,p}$) and ln($D_{i,q}$) data (i.e., $\beta_{Di,p}$ and $\beta_{Di,q}$), the demand correlation matrix is evaluated. Thereby, JDS against the i^{th} BS DS is generated using MATLAB [24] with the correlation matrix and the individual component demand distributions at that DS as the input.

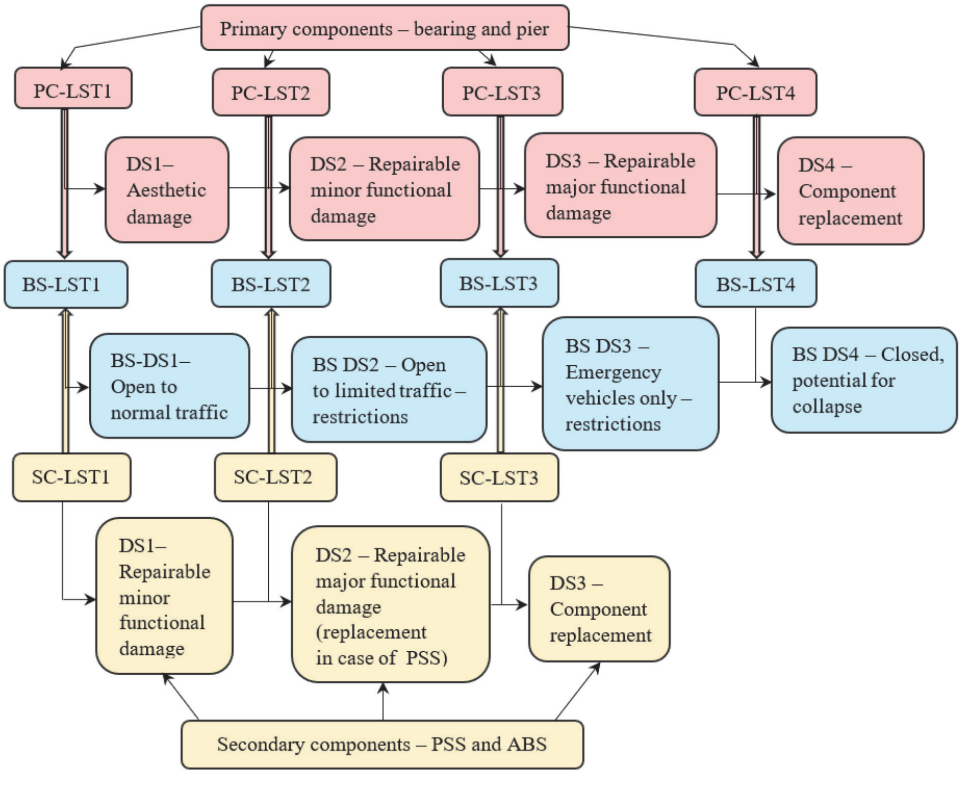

Figure 3. Descriptions of the DSs and mapping of the component-level DSs onto the BS DSs

$$\rho_{i,p-q} = \frac{\sum_{1296} \{\ln(D_{i,p}) - \overline{\ln(D_{i,p})}\}\{\ln(D_{i,q}) - \overline{\ln(D_{i,q})}\}}{\sqrt{\sum_{1296} \{\ln(D_{i,p}) - \overline{\ln(D_{i,p})}\}^2 \sum_{1296} \{\ln(D_{i,q}) - \overline{\ln(D_{i,q})}\}^2}} \quad (1)$$

Table 1. Correlation coefficients among the bridge component demands

DS1	IM	Value	DS2	IM	Value	DS3	IM	Value
$\rho_{1,pl\text{-}ab}$	*PGA*	0.938	$\rho_{2,pl\text{-}ab}$	*PGA*	0.914	$\rho_{3,ab\text{-}pr}$	*PGA*	0.697
	S_a(0.7s)	0.738		S_a(0.7s)	0.614		S_a(0.7s)	0.521
$\rho_{1,pl\text{-}pr}$	*PGA*	0.725	$\rho_{2,pl\text{-}pr}$	*PGA*	0.735	$\rho_{3,ab\text{-}pr}$	*PGA*	0.797
	S_a(0.7s)	0.216		S_a(0.7s)	0.468		S_a(0.7s)	0.493
$\rho_{1,pl\text{-}br}$	*PGA*	0.555	$\rho_{2,pl\text{-}br}$	*PGA*	0.781	$\rho_{3,br\text{-}pr}$	*PGA*	0
	S_a(0.7s)	0.250		S_a(0.7s)	0.328		S_a(0.7s)	0
$\rho_{1,ab\text{-}pr}$	*PGA*	0.683	$\rho_{2,ab\text{-}pr}$	*PGA*	0.777	DS4	*PGA*	S_a(0.7s)
	S_a(0.7s)	0.177		S_a(0.7s)	0.532			
$\rho_{1,ab\text{-}br}$	*PGA*	0.544	$\rho_{2,ab\text{-}pr}$	*PGA*	0.778	$\rho_{4,br\text{-}pr}$	0	0
	S_a(0.7s)	0.243		S_a(0.7s)	0.339			
$\rho_{1,br\text{-}pr}$	*PGA*	0.418	$\rho_{2,br\text{-}pr}$	*PGA*	0.786			
	S_a(0.7s)	0.487		S_a(0.7s)	0.916			

3.3 Computation of the system-level FC

Probability of reaching the i^{th} BS DS is obtained by comparing the joint demands of the components with the mutually independent component capacities *C*s (denoted as $C_{i,pl}$, $C_{i,ab}$, $C_{i,br}$, and $C_{i,pr}$ respectively for PSS, ABS, bearing and pier) at their respective i^{th} DSs, while assuming a series system failure. Employing LHST on the JDS and the individual *C* distributions, 102 samples for joint demands as well as individual component *C*s are obtained, while dividing each into 100 equal probability intervals and extracting the median values of the intervals along with the boundary values. Samples for the individual component *C*s are paired up randomly among them to have 102 quartets of *C*s. 102 joint demand sets are randomly paired with 102 capacity quartets. For a joint demand-capacity quartet pair, the BS DS is considered to have reached, if the *C* values are exceeded by the respective *D* values within the pair, at least for one component. The corresponding probability $P_{i,BS}$ is computed as the ratio of the number of pairs wherein the DS is reached to the total number of pairs (i.e., 102). Computation is repeated at each increasing value of both the adopted IMs and for all the BS DSs to obtain the corresponding BS FCs. The BS FC generation procedure is depicted in a flowchart, as in Fig. 4 and the generated BS FCs with respect to PGA and S_a(0.7s) are displayed in Figs. 5(a) and 5(b) respectively.

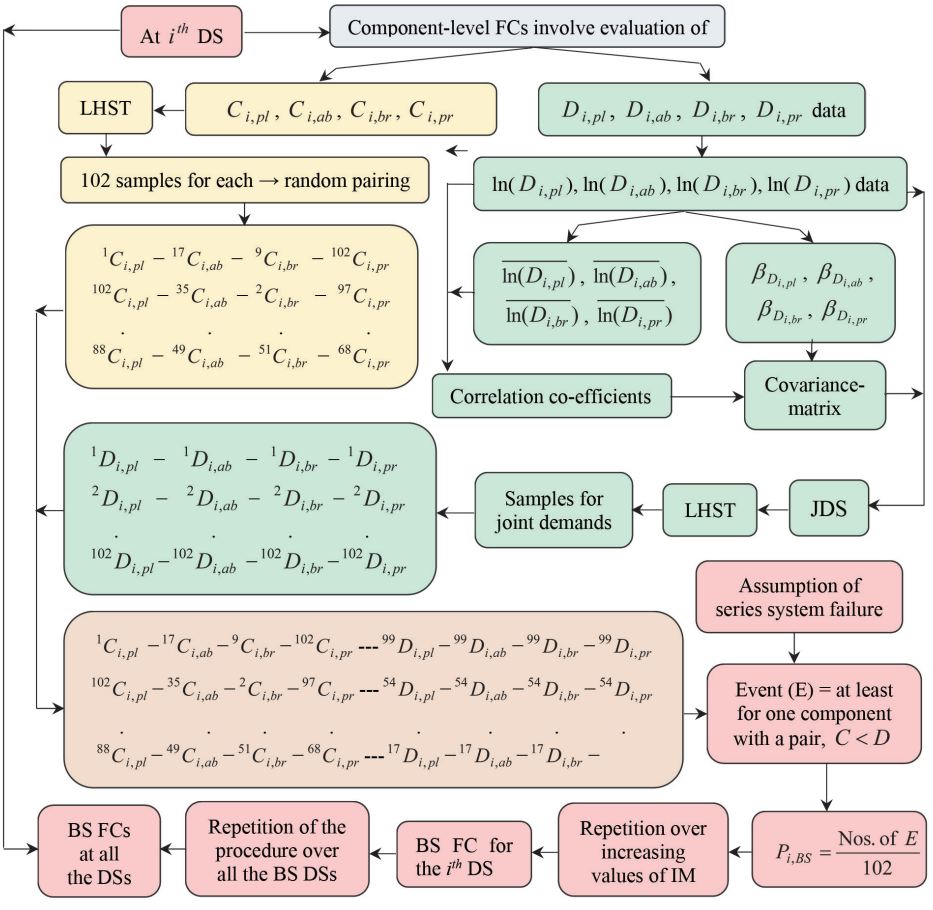

Figure 4. Flowchart describing the generation of the BS FCs

4 Comparison of the BS FCs with the individual component FCs and with respect to the adopted IMs

Vulnerability of the BS with respect to the individual components is examined through the comparisons of the respective FCs. BS is observed to be more vulnerable than all the components at the respective same DS rank, while at the DSs of higher ranks than those of the individual components, it shows more or less vulnerabilities upto certain ranges of IM and vice versa beyond as compared to the components. One such observation is shown in Fig. 5(c), displaying the differences in the generated FCs of the individual components at their respective DS1s with those of the BS at all its DSs, with respect to S_a(0.7s). Since, the differences between any two FCs vary with respect to IM, the comparisons are drawn as the percentage difference in fragility with respect to IM (δ)

between two FCs. BS at DS1 is observed to be more fragile than the most vulnerable one of all the components throughout the IM values; even at its DS2, BS is found to be more vulnerable than ABS, A-PSS and bearing at various IM values for this IAB class. Quantitatively, at the respective DS1s of the components and the BS, the maximum δ (δ_{max}) between the BS and A-PSS; BS and ABS; BS and bearing; BS and pier are observed to be 457 %; 452 %; 238 %; and 458 % at S_a(0.7s) values of 0.06g; 0.06g; 0.05g; and 0.06g respectively. At all its DSs, the BS FCs with respect to PGA show higher values as compared to those with respect to S_a(0.7s), as can be observed from Fig. 5(d) and Table 2 listing the respective δ_{max}.

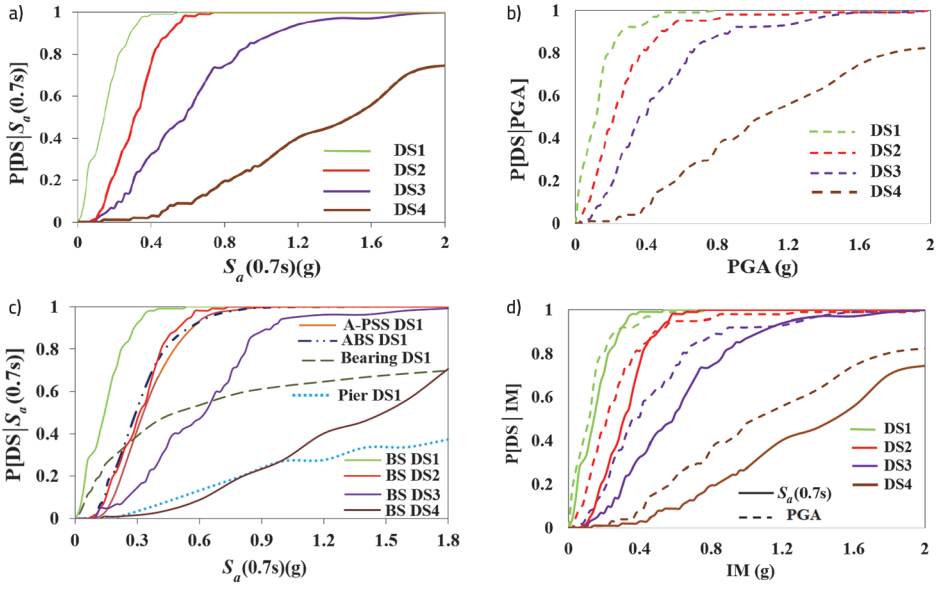

Figure 5. BS FCs with respect to a) PGA and b)S_a(0.7s); c) comparisons of BS FCs with respect to the individual components at the corresponding DS1s, and d) comparison between a) and b)

Table 2. Comparison of BS fragilities with respect to the IMs in the study

System-level FCs	DS1		DS2	
	IM value	δ_{max}	IM value	δ_{max}
PGA > S_a(0.7s)	≤ 0.30g	686 % (0.02g)	≤ 0.500g	161 % (0.14g)
PGA < S_a(0.7s)	> 0.30g	16 % (0.36g)	≤ 0.500g	7 % (0.74g)
System-level FCs	**DS3**		**DS4**	
	IM value	δ_{max}	**IM value**	δ_{max}
PGA > S_a(0.7s)	throughout	77 % (0.28g)	throughout	27 % (0.62g)

5 Conclusions

The present study derives the bridge system fragility curves for a class of reinforced concrete integral abutment bridges, in line with the current focus of the earthquake engineering research on the seismic vulnerability assessment of bridges. The bridge class constitutes multiple components, which are found to be vulnerable upto different degrees to various levels of the earthquake intensity measures taken as the peak ground acceleration (PGA) and spectral acceleration at time period of 7sec S_a(0.7s). Thus, the system fragility curves are derived by using the joint demand cumulative distribution surface generated from the correlated demands and the mutually independent capacity distributions of the individual components, assessed while evaluating the component-level fragility curves. Employing the Latin hypercube sampling techniques on the joint demands and the individual component capacities and assuming a series system assumption, the probability of reaching a bridge system damage state is obtained. Repetition of the procedure for each increasing level of both PGA and S_a(0.7s), and for all the bridge system damage states defined in the study, the respective fragility curves are derived. The salient conclusions drawn from the present study are:

Component-level demands show higher values with respect to PGA than S_a(0.7s) for most of the intensity measure levels. Consequently, for all the IAB components, fragilities estimated with respect to PGA are more than those with respect to S_a(0.7s) in most cases. This trend is also reflected in case of the bridge system fragility curves.

Degrees of correlations among the component demands assessed with respect to S_a(0.7s) are found to be less as compared to those obtained with respect to PGA at all DSs, except for the pier-bearing pair. Abutment backfill system and the pile soil system have the highest correlations in their demands among all the components, with respect to both PGA and S_a(0.7s); correlation slightly decreases with increasing DS rank. Correlations between pier and bearing demands increase significantly with the increasing DS ranks. However, these have zero correlations at higher damage states, owing to non-coexistence of their damage states together in any bridge system sample.

The three-span continuous reinforced concrete integral abutment bridge class is found to be more vulnerable as compared to all the individual components, at their respective damage states of the same ranks, as stated in a few past studies. Bridge system damage states of higher ranks either show more or less vulnerabilities upto certain ranges and vice versa beyond certain ranges of the intensity measure, with respect to the individual components.

Bridge system fragility curves generated with respect to PGA show maximum deviation from those with respect to S_a(0.7s) at the bridge system first damage state, which decrease with the increasing damage state rank; also, the point where the peak deviation occurs within a curve shifts to a higher intensity measure value. These trends follow similar patterns, as observed for all the components.

BS FCs evaluated, while incorporating the amount of correlations existing among the component demands, are expected to be more reliable rather than using the traditional series or parallel combination philosophy for the bridge component fragilities which might lead to their possible underestimation or overestimation.

References

[1] Song, J., Kang, W.H. (2009): System reliability and sensitivity under statistical dependence by matrix-based system reliability method. Structural Safety, 31 (2), 48-156.

[2] Choi, E., DesRoches, R., Neilson, B. (2004): Seismic fragility of typical bridges in moderate seismic zones. Engineering Structures, 26, 187–199.

[3] Taskari, O., Sextos, A. (2015): Multi-angle, multi-damage fragility curves for seismic assessment of bridges. Earthquake Engineering and Structural Dynamics, 44 (13), 2281-2301

[4] Karim, K.R., Yamazaki, F. (2001): Effect of earthquake ground motions on fragility curves of highway bridges piers based on numerical simulation. Earthquake Engineering and Structural Dynamics, 30, 1839–1856.

[5] Shinozuka, M., Feng, M.Q., Kim, H., Uzawa, T., Ueda, T. (2001): Statistical Analysis of Fragility Curves. Technical Report MCEER, University of Southern California.

[6] Kunnath, S.K., Larson, L., Miranda, E. (2006): Modelling considerations in probabilistic performance-based seismic evaluation: case study of the I-880 viaduct. Earthquake Engineering and Structural Dynamics, 35, 57–75.

[7] Banerjee, S., Shinozuka, M. (2008): Mechanistic quantification of RC bridge damage states under earthquake through fragility analysis. Probabilistic Engineering Mechanics, 23 (1), 12-22.

[8] Zhong, J., Gardoni, P., Rosowsky, D., Haukaas, T. (2008): Probabilistic Seismic Demand Models and Fragility Estimates for Reinforced Concrete Bridges with Two-Column Bents. Journal of Engineering Mechanics, 134, 495-504.

[9] Nielson, B.G., DesRoches, R. (2007): Seismic fragility methodology for highway bridges using component level approach. Earthquake Engineering and Structural Dynamics, 36 (6), 823-839.

[10] Pan, Y., Agrawal, A.K., Ghosn, M. (2007): Seismic Fragility of Continuous Steel Highway Bridges in New York State. Journal of Bridge Engineering, 12, 689-699.

[11] Zhang, J., Huo, Y. (2009): Evaluating effectiveness and optimum design of isolation devices for highway bridges using fragility function method. Engineering Structures, 31 (8), 1648–1660.

[12] Mackie, K., Stojadinovic, B. (2005): Fragility basis for California highway overpass bridge seismic decision making. Pacific Earthquake Engineering Research Center, College of Engineering, University of California, Berkeley.

[13] Nielson, B.G. (2005): Analytical Fragility Curves for Highway Bridges in Moderate Seismic Zones. Ph.D. Thesis, School of Civil and Environmental Engineering, Georgia Institute of Technology.

[14] Padgett, J., DesRoches, R. (2009): Retrofitted bridge fragility analysis for typical classes of multi-span bridges. Earthquake Spectra, 25 (1), 117–141.

[15] Kwon, O.S., Elnashai, A.S. (2010): Fragility analysis of a highway over-crossing bridge with consideration of soil–structure interactions. Structure and Infrastructure Engineering, 6 (1-2), 159–178.

[16] Ramanathan, K.N. (2012). "Next generation seismic fragility curves for California bridges incorporating the evolution in seismic design philosophy," Ph.D. Thesis, Georgia Institute of Technology.

[17] Zakeri, B., Padgett, J.E., Amiri, G.G. (2014): Fragility analysis of skewed single-frame concrete box-girder bridges. Journal of Performance of Constructed Facilities, 28 (3), 571-582.

[18] Priestley, M.J.N., Seible, F., Calvi, G.M. (1996): Seismic Design and Retrofit of Bridges. John Wiley and Sons, New York.

[19] McKenna, F., Fenves, G.L., Scott, M.H. (2000): Open System for Earthquake Engineering Simulation. OpenSees Command Manual. University of California, Berkeley, California.

[20] Ashour, M., Norris, G. (2000): Modeling lateral soil-pile response based on soil-pile interaction. Journal of Geotechnical and Geoenvironmental Engineering, ASCE, 126 (5), paper no.19113, 420-428.

[21] Shamsabadi, A., Ashour, M., Norris, G. (2005) "Bridge Abutment Nonlinear Force-Displacement Capacity Prediction for Seismic Design." Journal of Geotechnical and Geoenvironmental Engineering, 131(2), 151-161.

[22] Ahmed, B.F., Dasgupta, K. (2020). "Component Level Seismic Fragility Assessment of Multispan Continuous Integral Abutment Bridges." 17thWorld Conference on Earthquake Engineering, 17WCEE, Sendai, Japan, 13-18 September, Paper No. 3c-0007.

[23] Cardone, D., Perrone, G., Dolce, M. (2007): Seismic risk assessment of highway bridges. 1st US–Italy Seismic Bridge Workshop, IUSS Press Ltd, Pavia (Italy).

[24] MATLAB 8.6 (2015): MATLAB: Language of Technical Computing. MathWorks, New York, NY, R2015b edition.